Journal of Power Sources 188 (2009) 286–291

Contents lists available at ScienceDirect

Journal of Power Sources

journal homepage: www.elsevier.com/locate/jpowsour

Electrochemical reactivity of ball-milled MoO_{3-y} as anode materials for lithium-ion batteries

Yoon S. Jung[a], Sangkyoo Lee[a], Dongjoon Ahn[a], Anne C. Dillon[b], Se-Hee Lee[a,*]

[a] Department of Mechanical Engineering, University of Colorado at Boulder, Boulder, CO 80309-0427, USA
[b] National Renewable Energy Laboratory, Golden, CO 80401, USA

ARTICLE INFO

Article history:
Received 6 November 2008
Received in revised form
22 November 2008
Accepted 24 November 2008
Available online 6 December 2008

Keywords:
Li-ion batteries
Metal oxide
Ball-milling
Nanostructure
Conversion reaction
Reactivity

ABSTRACT

The electrochemical reactivity of ball-milled MoO_3 powders was investigated in Li rechargeable cells. High-energy ball-milling converts highly-crystalline MoO_3 bulk powders into partially reduced low-crystalline MoO_{3-y} materials with a reduced particle size. Both bulk and ball-milled MoO_3 exhibit a first discharge capacity beyond 1100 mAh g^{-1} when tested in the 0–3 V (*vs.* Li/Li^+) range, which is indicative of a complete conversion reaction. It is found that partial reduction caused by ball-milling results in a reduction in the conversion reaction. Additionally, incomplete re-oxidation during subsequent charge results in the formation of MoO_2 instead of MoO_3, which in turn affects the reactivity in subsequent cycles. As compared to bulk MoO_3, ball-milled MoO_{3-y} showed significantly enhanced cycle performance (bulk: 27.6% charge capacity retention at the 10th cycle *vs.* ball-milled for 8 h: 64.4% at the 35th cycle), which can be attributed to the nano-texture wherein nanometer-sized particles aggregate to form secondary ones.

1. Introduction

As the environmental challenge of global warming resulting from fossil-fuel consumption is growing more severe, the importance of electrochemical energy conversion/storage devices cannot be overemphasized. Among them, rechargeable lithium-ion batteries (LIB) have been widely used in various portable electronic devices. Even further, thanks to their superior performance to the other competitors such as Ni-MH batteries, their development for hybrid electric vehicles (HEV), plug-in hybrid electric vehicles (PHEV), or all electric vehicles is a current focus.

For successful application, however, electrode materials that can meet the following requirements should be developed: high-energy density, longer cycle life, high power, and safety with low cost. Regarding high capacity, conversion-type transition metal oxides (MO with M = Fe, Co, Ni, Cu, Ru, etc., $MO + Li^+ + e^- \leftrightarrow Li_2O + M$) may have a capacity as high as 700 mAh g^{-1} (e.g. CoO: 715 mAh g^{-1}) which is much higher than that of already-commercialized graphite (372 mAh g^{-1}) [1–6]. Furthermore, many transition metal oxides show outstanding cycling performance [1,6,7–9]. And for the purpose of more improved cycle retention, various synthetic strategies to develop nanostructure have been employed [7–9]. On the aspect of high power, the nanostructure can also significantly enhance the rate capability by reason of shortened diffusion length [7,9,10]. Hence, the nanostructured transition metal oxides can be regarded as one of the most promising candidate materials.

MoO_x which can be also categorized as one of the conversion-type transition metal oxides has additional advantageous features of low cost and environmental benignity as well as even higher capacity. To date, various preparation methods of nanostructured MoO_x and their corresponding electrochemical performance have been reported. Among them, one can quote the fissile MoO_2 by hydrothermal reaction [11,12], the porous spherical MoO_2 by rheological phase reaction [12], the α-MoO_3 micro-rods by vapor-transportation method [13], the carbon/MoO_2 composite using tri-block copolymer as a structure directing agent and carbon source [14], MoO_3 nanobelts by hydrothermal reaction [15] and utilizing poly(ethylene glycol) [16], MoO_2 by reduction of MoO_3 with ethanol vapor [17], MoO_3 nanoparticles by hot-wire chemical vapor deposition (HWCVD) [18,19], tremella-like MoO_2 by hydrothermal reduction [20], etc. However, most research about MoO_x as an anode in the potential range down to 0 V (*vs.* Li/Li^+) has focused on MoO_2 rather than MoO_3 even though MoO_3 can theoretically accommodate more Li (six Li) than MoO_2 (four Li) (MoO_3: 1117 mAh g^{-1}, MoO_2: 838 mAh g^{-1}). Thus, the electrochemical reactivity of MoO_3 utilizing a conversion reaction has not yet been fully investigated. Moreover, for the case of MoO_2, their reaction is known to be restricted to the addition-type one ($MO_y + xLi^+ + xe^- \leftrightarrow Li_xMO_y$, no breakage of M–O bond) at room temperature without using nanostructured electrodes [11,17,21,22].

* Corresponding author. Tel.: +1 303 492 7889; fax: +1 303 492 3498.
E-mail address: sehee.lee@colorado.edu (S.-H. Lee).

0378-7753/$ – see front matter © 2008 Elsevier B.V. All rights reserved.
doi:10.1016/j.jpowsour.2008.11.125

Here we report the electrochemical performance of ball-milled MoO_3 powders. High-energy ball-milling is one of the easiest ways to construct nanostructures [23–25]. The composition, morphology, and structure of ball-milled MoO_3 have been characterized and their effects on the electrochemical reactivity and extent of conversion reaction are discussed.

2. Experimental

2.1. Preparation

Milling was performed using SPEX 8000 Mixer/Mill. The MoO_3 powders (Alfa Aesar, 3 g) as well as steel balls (two balls of 1.3 cm in diameter and six balls of 0.6 cm in diameter) were put into a hardened steel vial (72 cm^3). The weight ratio between the steel ball and the MoO_3 powders was 9:1. Three different ball-milled samples were prepared by ball-milling bulk MoO_3 powders for 4, 6, and 8 h.

2.2. Characterization of materials

A Phillips CM-30 TEM operating at 200 kV with a 50 μm objective aperture for improved contrast was employed for an extensive TEM analyses. X-ray diffraction (XRD) patterns were recorded using Scintag PTS 4-circle goniometer (Bragg–Brentano geometry) using Cu K_α radiation (1.54056 Å) generated at 45 kV and 36 mA and detected with a liquid-nitrogen-cooled solid-state germanium detector. Using inductively coupled plasma atom emission spectroscopy (ICP-AES, ARL 3410+), oxygen deficiency was determined by measuring Mo content. After the known amount of MoO_{3-y} powders were completely dissolved in concentrated sulphuric acid at 95 °C over 4 h, the concentration of Mo was measured.

2.3. Electrochemical characterization

A two-electrode 2032-type coin cell was employed to assess the electrochemical performance of samples. The composite electrodes were prepared by spreading a slurry mixture of MoO_{3-y} powders, acetylene black (carbon additive for conductivity enhancement), and poly(vinylidine fluoride) (PVDF) (8:1:1, wt. ratio) on a piece of Cu foil and were dried. The dried electrodes were then heat-treated at 250 °C under Ar atmosphere overnight to improve the electrochemical performance [26,27]. Li foil (Alfa Aesar) was used as the counter and reference electrode. 1.0 M $LiPF_6$ dissolved in a mixture of propylene carbonate (PC) and dimethyl carbonate (DMC) (1:1, v/v) was used as the electrolyte. The galvanostatic discharge–charge cycling was made in the potential range of 0–3 V (*vs.* Li/Li^+) at 55 μA cm^{-2} (0.03*C*-rate, theoretically 1*C*-rate = 1117 mA g^{-1}). As the separator, porous polypropylene (PP)/polyethylene (PE)/PP tri-layer film was used. Cells were assembled in an Ar-filled dry box and cycled at room temperature. In this report, lithiation was expressed as discharging and de-lithiation as charging because Li foil was used as the counter electrode in the half-cells.

3. Results and discussion

3.1. Materials characterization

Fig. 1 shows the TEM images of bulk and ball-milled MoO_3 powders. Different from bulk MoO_3 powders (Fig. 1a), the ball-milled MoO_{3-y} powders (Fig. 1b–d) exhibit roughened surface morphology as well as slightly reduced overall particle size (approx. 1 μm). The enlarged views (the inset in Fig. 1b and c) reveal that the overall particles of ball-milled samples consist of agglomerated nanometer-sized primary particles. Intense collisions between particles and balls during the high-energy ball-milling can both cause the particles to fracture and also to become welded to each other [23–25]. The observed nano-crystalline-aggregation for ball-milled MoO_3 powders results from this combined breaking/welding mechanism.

In order to identify crystalline structure and estimate the extent of crystallinity, XRD patterns of the bulk and ball-milled MoO_{3-x} powders (Fig. 2) were obtained. The sharp characteristic peaks for both bulk and ball-milled MoO_3 powders correspond well with orthorhombic α-MoO_3 (JCPDS no. 05-0508). The orthorhombic α-MoO_3 is known to have a layered structure (parallel to (0 1 0)), where layers are bound to each other by van der Waals interactions [13,15]. Three strong peaks corresponding to (0 2 0), (0 4 0), and (0 6 0) planes for the bulk MoO_3 powder, indicate the formation of the anisotropic layered structure [15]. As the MoO_3 powders are ball-milled, two major changes are noticeable. First, the peak ratios match with that of standard orthorhombic α-MoO_3. This indicates that the intense breakage of particles during ball-milling removes the anisotropy [24]. Second, more importantly, the diffraction peaks are significantly broadened indicating appreciably reduced crystallite size and/or lowered crystallinity. This feature agrees well with the observation of the nano-crystalline-aggregations in the TEM analyses (insets of Fig. 1b and c).

In addition to the morphological (Fig. 1) and crystalline structural (Fig. 2) changes, high-energy ball-milling also changes the chemical composition. Using ICP-AES analyses, the oxygen contents of ball-milled MoO_3 powders were determined and are plotted in Fig. 3. The bulk MoO_3 powders were partially reduced to give $MoO_{2.929}$, $MoO_{2.903}$, and $MoO_{2.895}$ by ball-milling for 4, 6, and 8 h, respectively. Oxygen deficiency gradually increases as the ball-milling time increases.

3.2. Electrochemical reactivity of ball-milled MoO_{3-x} powders

The first and second discharge–charge voltage profiles of bulk and ball-milled MoO_{3-x} powders are shown in Fig. 4. The vertical lines indicate the theoretical limits for MoO_{3-x} electrodes that undergo a complete conversion reaction to produce Mo metal and lithia (Li_2O). The slightly decreased theoretical Li-uptake limit (vertical lines) for ball-milled samples as compared to the bulk sample is due to the reduced oxygen contents in the partially reduced particles. For both bulk and ball-milled MoO_{3-y}, all of the first lithiation capacities exceed the theoretical limit, which confirms that the conversion reaction is complete. It is noticeable that bulk MoO_3 exhibits complete conversion reaction as opposed to MoO_2 which is known to be restricted to the addition reaction [11,17,21,22]. This difference can be explained by thermodynamic and kinetic consideration. Thermodynamically, the Gibbs free energy of formation is a good indicator of how much MoO_x will undergo a favorable conversion-type lithiation reaction. The less negative value of MoO_3 (−186.3 kJ (g atom)$^{-1}$) than that of MoO_2 (−196.0 kJ (g atom)$^{-1}$) gives a higher lithiation equilibrium potential following reactions (1) and (2) [28]:

$$MoO_3 + 6Li^+ + 6e^- \rightarrow Mo + 3Li_2O \quad (E_{eq,1}{}^\circ = 1.83\,V(vs.Li/Li^+)) \quad (1)$$

$$MoO_2 + 4Li^+ + 4e^- \rightarrow Mo + 2Li_2O \quad (E_{eq,2}{}^\circ = 1.60\,V(vs.Li/Li^+)) \quad (2)$$

However, it should be noted that the conversion reactions are thermodynamically feasible for both MoO_2 and MoO_3. From the reaction kinetics point of view, the conversion-type transition metal oxides are known to suffer from a large lithiation overpotential [7,10,27,29], which is believed to stem from the high activation energy for breaking M–O bonds upon lithiation [30–34]. Due to the lower equilibrium potential (smaller driving force) in addition to a large activation barrier, the lithation reactivity of MoO_2 is limited to the addition reaction.

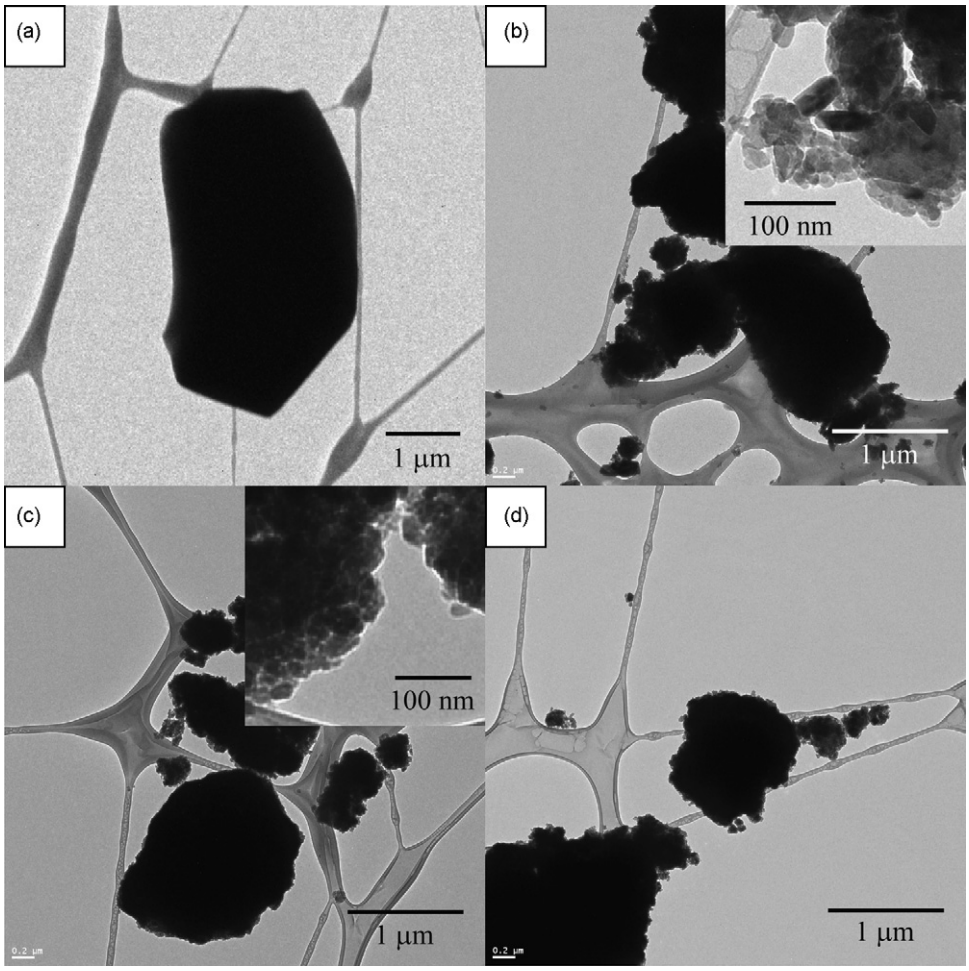

Fig. 1. TEM images of MoO_{3-y} powders. (a) Bulk powders and powders ball-milled for (b) 4 h, (c) 6 h, and (d) 8 h. Enlarged views are given in the inset.

In the case of bulk MoO_3 in Fig. 4, the first lithiation reaction can be divided into two regions: Region I up to 1.5 V (*vs.* Li/Li^+) and Region II below 0.5 V. In region I, approximately 1.2 Li is inserted with two discrete plateaus (at 2.7 and 2.3 V). This high-voltage reaction agrees well with previous reports in which it is claimed that slightly more than one Li can be accommodated in the interlayer spacing between the Mo–O octahedron layers and Mo–O octahedron intralayers [13,15,16]. As the potential decreases to region II, a long plateau at 0.45 V followed by the sloping profile below 0.3 V develops, which is commonly encountered in most conversion-type transition metal oxides [1–10,27]. The former long plateau is consistent with the additional 4.8 Li uptake for the complete conversion reaction. There are two different possible mechanisms to explain the latter sloping profile, which is primarily attributed to the Li

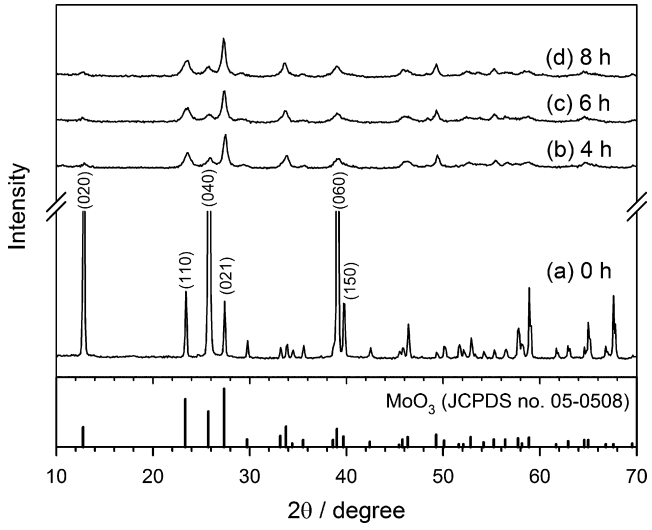

Fig. 2. XRD patterns of MoO_{3-y} powders. Ball-milling time is given in the inset.

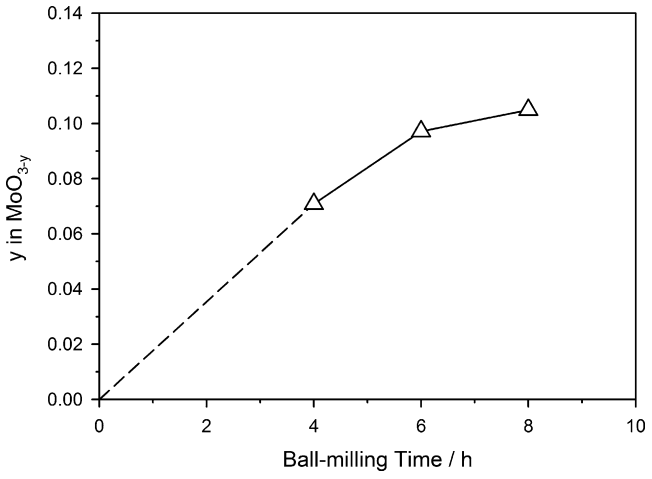

Fig. 3. Oxygen-deficiency of ball-milled MoO_{3-y} powders.

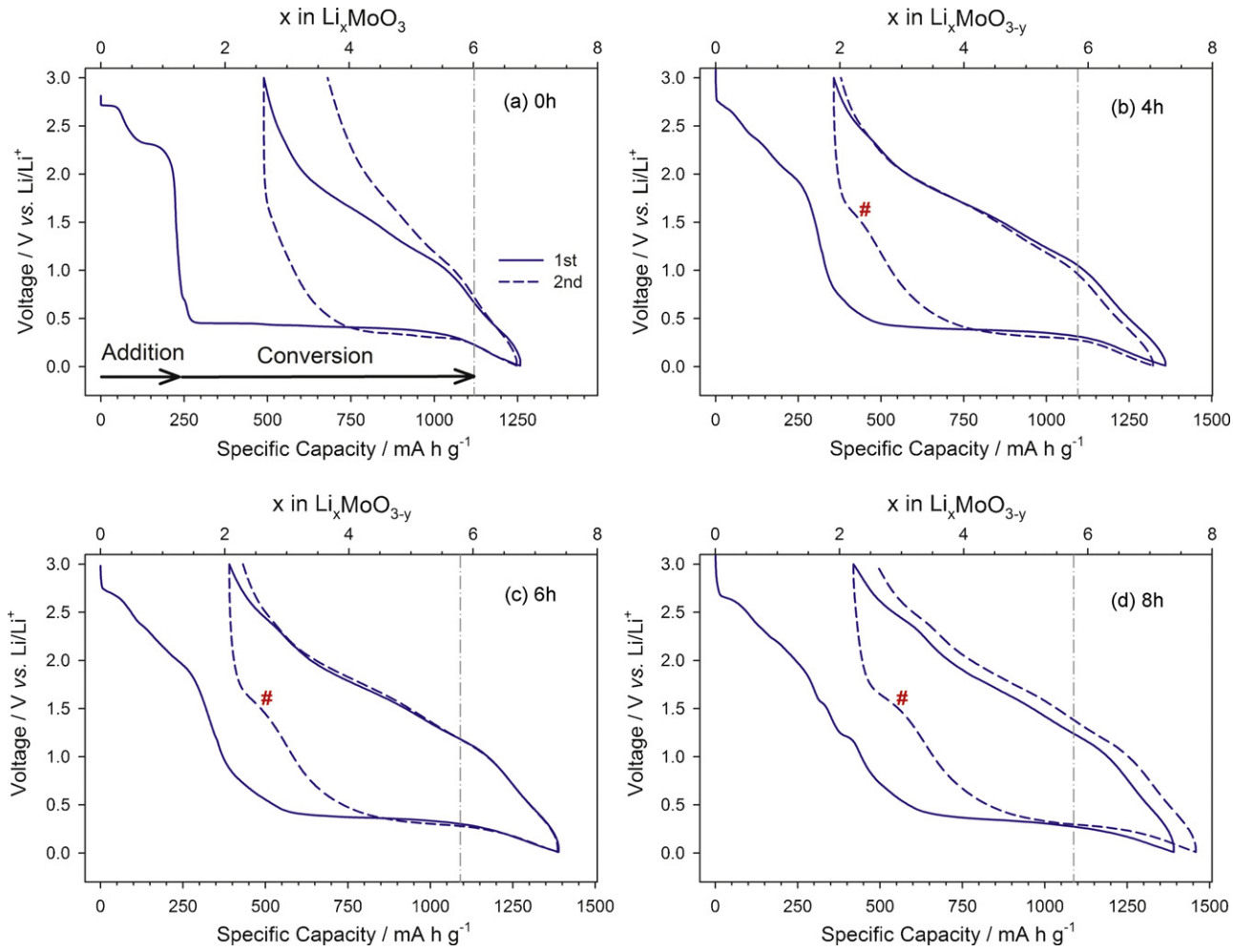

Fig. 4. First and second discharge–charge voltage profiles of MoO_{3-y} electrodes. Ball-milling time is given in the inset. Vertical lines indicate the expected capacity for a full reduction of MoO_{3-y} ($MoO_{3-y} + 2(3-y)Li^+ + 2(3-y)e^- \rightarrow (3-y)Li_2O + Mo$).

capacity extending beyond the theoretical limit: (i) Tarascon and co-workers ascribed the sloping region mainly to the formation of a polymer-like organic layer catalyzed by in-situ formed nanoparticles [35,36]. Using X-ray photoelectron spectroscopy (XPS), they show the evidence of growth of both an inorganic (mainly Li_2CO_3 and alkyl carbonates) and an organic layer (poly(ethylene oxide) oligomers) during lithiation, which is not directly related to the conversion reaction ($MO_x + xLi^+ + xe^- \rightarrow M + xLi_2O$). And the organic layer is found to be partially vanishing upon cycling, which implies this reaction could be attributed to additional reversible capacity. (ii) Maier and co-workers proposed an interfacial storage mechanism [37,38]. Except for the surface-related reaction (formation of polymer-like organic layer or interfacial storage in region II), the overall first lithiation reaction for bulk MoO_3 can be expressed as follows Eqs. (3) and (4):

$$\text{Addition}(>1.5\,\text{V}): \quad MoO_3 + xLi^+ + xe^- \rightarrow Li_xMoO_3 \quad (x = \sim 1.2) \tag{3}$$

$$\text{Conversion}(<0.5\,\text{V}): \quad Li_xMoO_3 + (6-x)Li^+ + (6-x)e^- \rightarrow Mo + 3Li_2O \tag{4}$$

From the comparison of the first discharge profiles of ball-milled MoO_{3-y} to that of the bulk MoO_3, one can expect that the ball-milled MoO_{3-y} powders also follow the above reaction pathway (Eqs. (3) and (4)) although their voltage profiles become smoother than that of the bulk MoO_3. The smoother voltage profile can be explained in terms of the surface energy described for many nanosystems [37,39–41], and unequivocally reveal the nanostructural nature of ball-milled MoO_{3-y} powders. Regarding the first discharge capacity, the Li uptake increases as the ball-milling time increases as seen in Fig. 5 (squares). The discharge capacity is

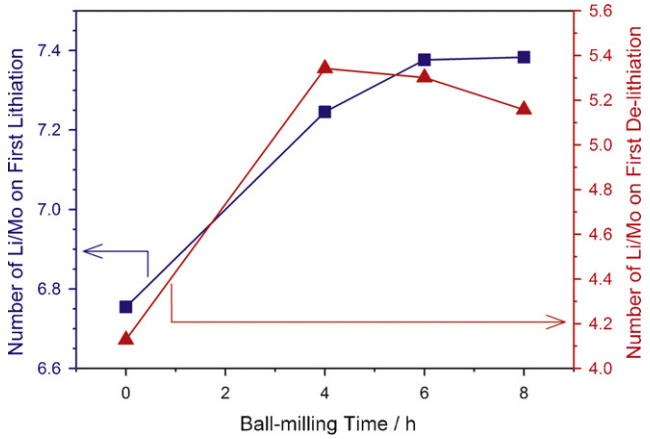

Fig. 5. Number of inserted/de-inserted Li/Mo for MoO_{3-y} electrodes on the first lithiation and de-lithiation according to the ball-milling time.

determined from the amount of Li_2O formation and the additional decomposition reaction of the electrolyte on the electrode surface. The higher discharge capacity for MoO_{3-y} powders ball-milled for longer time in spite of their lower oxygen contents indicates that surface-related decomposition reaction is a more dominant factor than oxygen deficiency.

After the full conversion reaction, the extracted Mo metal is re-oxidized by Li_2O with a voltage slope during charge as displayed in Fig. 4. However, the remaining Li after the first full charge corresponds to ~2.5 and ~2 Li/Mo for the bulk and ball-milled MoO_3, respectively. Moreover, the amount of extracted Li during the first charge (triangles in Fig. 5) does not reach six Li/Mo for any of the materials. These two observations imply that the Mo metal is not fully recovered but partially re-oxidized to produce mainly MoO_2 with residual Li_2O. The variation in the first charge capacity provides very interesting information. First, the charge capacity for ball-milled MoO_{3-y} is significantly enhanced as compared to the bulk MoO_3, showing that the nano-texturing for ball-milled samples enhances the electrochemical reversibility. Second, for ball-milled MoO_{3-y}, the amount of extracted Li decreases as ball-milling time increases. This is not a surprising behavior because MoO_{3-y} ball-milled for longer time gives less Li_2O after conversion reaction and thus Mo with less Li_2O will be oxidized less.

Once the conversion reaction proceeds completely, the re-oxidized transition metal oxide phases are known to have amorphous structure resulting in smoother lithiation voltage profiles in the subsequent cycles [1,6,9,10,35,42]. The smoother lithiation voltage profile in the second cycle for the bulk MoO_3 (Fig. 4a) is consistent with the amorphization.

Fig. 6 displays the differential discharge capacity profiles for the first and second cycles. Again, two peaks at 2.7 and 2.3 V (*vs.* Li/Li^+) are assigned to an addition reaction while the peaks ('*' and '^') in the 0.3–0.5 V range are due to the conversion reaction. For the conversion reaction, there are several important features to be pointed out. First, as ball-milling time increases, the peaks broaden, which is indicative of a nano-size effect [37,39–41]. Second, the conversion reaction peaks in the first cycle for ball-milled MoO_{3-y} significantly shifts toward the negative direction. This shift can be explained in terms of chemical composition rather than crystallite size or crystallinity. As shown in Fig. 3, ball-milling induces partial reduction, and ball-milling for longer time results in more reduced MoO_{3-y}. Considering that MoO_2 can be regarded as the ultimate composition of partially reduced MoO_{3-y}, it may be assumed that partially reduced MoO_{3-y} should have intermediate reactivity between MoO_3 and MoO_2 which has limited reactivity for the conversion reaction at room temperature. According to this assumption, lower reactivity or appearance of conversion peaks for ball-milled MoO_{3-y} at lower potential than bulk MoO_3 can be explained by this oxygen-deficiency effect. Overall, it is prudent to say that the conversion reaction for ball-milled MoO_{3-y} depends more strongly on oxygen deficiency rather than the crystallite size or crystallinity. The similar reasoning can be applied to explain why the conversion peaks in the second cycle appear at even lower potential than those in the first cycle. In common cases for transition metal oxides, the second conversion reaction takes place at a higher potential than in the first cycle [1,4,6,9,10,27,36,42,43], which is explained by kinetically more favorable Li^+ and O^{2-} diffusion in the amorphized structure [29] and/or increased lithiation equilibrium potential from a thermodynamic point of view [42]. Consistent with the lower reactivity of MoO_2 than MoO_3 toward conversion reaction, the conversion peaks ('^') in the second cycle appear at even a lower potential than that ('*') of the first cycle strongly suggesting that re-oxidation is not completed but rather that the MoO_2 phase is formed. This is also supported by a smooth plateau ('#') around 1.5 V (*vs.* Li/Li^+) in the second

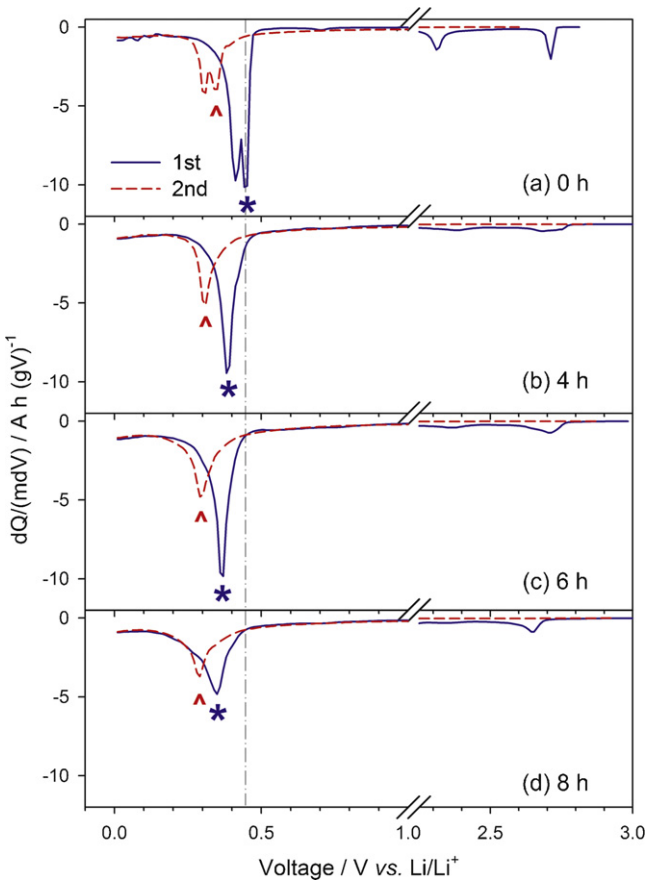

Fig. 6. Differential discharge capacity profiles for the first two cycles. Ball-milling time is given in the inset. Note that the first lithiation peaks ('*') for ball-milled MoO_{3-y} electrodes are negatively shifted from that for bare MoO_3 one and the second peaks ('^') for all electrodes are even more negatively shifted.

lithiation voltage profiles observed in Fig. 4 because this reaction potential corresponds to that for the addition reaction of MoO_2 [21,22].

Fig. 7 compares the cycle performance of bare and ball-milled MoO_{3-y} electrodes. Compared to the bulk MoO_3, the ball-milled MoO_{3-y} exhibits significantly enhanced cycle retention. In order to explain this, the large volume change that occurs for many

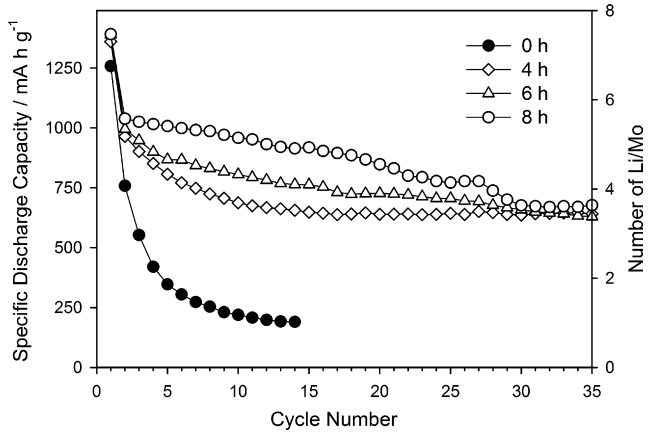

Fig. 7. Cycle performance of MoO_{3-y} electrodes. Ball-milling time is given in the inset. Number of inserted Li/Mo on the right axis is calculated based on the stoichiometric MoO_3.

conversion-type transition metal oxides during discharge–charge is considered ($(V_f - V_i)/V_i$, e.g. CoO: 73%, FeO: 106%, NiO: 121%).[1] The volume change has previously been considered only to a limited extent [27]. For MoO_3, the volume change is calculated to be as much as 104%.[2] As Li-alloy materials such as Si suffer from even more extreme volume changes, failure mechanisms and strategies associated with Li-alloy materials can provide us with important information. For Li-alloy materials, as lithiation proceeds, electrode particles become swollen. On the contrary, upon de-lithiation, swollen lithiated particles shrink, and the electronic contacts between particles become loose. Then, some fraction of electrode particles that lose their electronic path remains in the lithiated state and act as 'dead' particles even if the electrode is fully charged [44–46]. This is the main failure mode for most Li-alloy materials. Using nano-sized particles and/or employing an amorphous phase rather than a crystalline phase are well known strategies to improve cycle retention. The failure modes and factors to affect cycle retention in Li-alloy materials could be applied to the case of MoO_3. Based on this mechanism, the best cycle performance of the MoO_{3-y} powder ball-milled for the longest time (8 h) can be attributed to the smallest crystallite size and/or the lowest crystalline nature. It is also interesting to note that the capacity of ball-milled MoO_{3-y} converges close to ~4 Li/Mo around 30th cycle, which indicates that red/ox reaction be restricted to MoO_2/Li_2O. This phenomenon is consistent with the difficult oxidation from MoO_2 to MoO_3: as the electrode degrades and loses electronic conductivity among particles and/or domains, further oxidation from MoO_2 to MoO_3 can be expected to be even worse. Within this context, uniform coating of nano-sized MoO_3 with electronic and ionic conductors such as carbon could improve the reversibility as well as cycle retention. Further, this approach could prevent dissolution which is also considered as origin of capacity fade for long-term cycles in the conversion-type transition metal oxides [36].

4. Conclusion

Nanostructured MoO_{3-y} powders have been prepared by ball-milling, and their electrochemical reactivity in the 0–3 V (*vs.* Li/Li^+) range has been studied. Ball-milling of MoO_3 powders results in partially reduced MoO_{3-y} powders that consist of nano-crystallite aggregates. Bulk and ball-milled MoO_{3-y} can uptake more than six Li/Mo by an addition reaction followed by a conversion reaction, wherein the reactivity was found to strongly depend on the oxygen deficiency. The conversion reaction for highly-reduced MoO_{3-y} takes place at lower potential. However, the re-oxidation reactions are not complete, which can be rationalized from the inability of MoO_2/Li_2O to form MoO_3. This incomplete re-oxidation was found to affect the reversibility in the subsequent cycles. As compared to bulk MoO_3, ball-milled MoO_{3-y} shows significantly improved cycle retention, which can be attributed to the smaller crystallite size and/or low crystalline nature.

Acknowledgements

This work was funded by the U.S. Department of Energy under subcontract number DE-AC36-99-GO10337 through the Office of Energy Efficiency and Renewable Energy Office of the Vehicle Technologies Program. Dr. Yoon S. Jung acknowledges the Korea Research Foundation Grant funded by the Korean Government [KRF-2008-357-D00066]. Sangkyoo Lee acknowledges the Korea South-East Power Generation Co.

[1] V_i: initial volume of metal oxide (MO). V_f: final volume after full conversion reaction (M/Li_2O). Following specific densities ($g\,cm^{-3}$) were used to calculate volume change; CoO: 5.305 (JCPDS no. 42-1300), FeO: 5.973 (JCPDS no. 06-0615), NiO: 6.808 (JCPDS no. 4-1159), Co: 8.798 (JCPDS no. 15-0806), Fe: 7.875 (JCPDS no. 06-0696), Ni: 8.911 (JCPDS no. 04-0850), Li_2O: 2.204 (JCPDS no. 12-0254).

[2] Following specific density ($g\,cm^{-3}$) were used to calculate volume change; MoO_3: 4.710 (JCPDS no. 05-0508), Mo: 10.221 (JCPDS no. 42-1120).

References

[1] P. Poizot, S. Laruelle, S. Grugeon, L. Dupont, J.-M. Tarascon, Nature 407 (2001) 496.
[2] A. Débart, L. Dupont, P. Poizot, J.-B. Leriche, J.-M. Tarascon, J. Electrochem. Soc. 148 (2001) A1266.
[3] P. Poizot, S. Laruelle, S. Grugeon, J.-M. Tarascon, J. Electrochem. Soc. 149 (2002) A1212.
[4] D. Larcher, G. Sudant, J.-B. Leriche, Y. Chabre, J.-M. Tarascon, J. Electrochem. Soc. 149 (2002) A234.
[5] D. Larcher, D. Bonnin, R. Cortes, I. Rivals, L. Personnaz, J.-M. Tarascon, J. Electrochem. Soc. 150 (2003) A1643.
[6] P. Balaya, H. Li, L. Kienle, J. Maier, Adv. Funct. Mater. 13 (2003) 621.
[7] F. Jiao, J. Bao, P.G. Bruce, Electrochem. Solid-State Lett. 10 (2007) A264.
[8] M.V. Reddy, T. Yu, C. Sow, Z.X. Shen, C.T. Lim, G.V.S. Rao, B.V.R. Chowdari, Adv. Funct. Mater. 17 (2007) 2792.
[9] Y. Sharma, N. Sharma, G.V.S. Rao, B.V.R. Chowdari, Adv. Funct. Mater. 17 (2007) 2855.
[10] L. Taberna, S. Mitra, P. Poizot, P. Simon, J.-M. Tarascon, Nat. Mater. 5 (2006) 567.
[11] Y. Liang, S. Yang, Z. Yi, X. Lei, J. Sun, Y. Zhou, Mater. Sci. Eng. B 121 (2005) 152.
[12] Y. Liang, S. Yang, Z. Yi, J. Sun, Y. Zhou, Mater. Chem. Phys. 93 (2005) 395.
[13] W Li, F. Cheng, Z. Tao, J. Chen, J. Phys. Chem. B 110 (2006) 119.
[14] X. Ji, P. Subramanya, Y. Rho, L.F. Nazar, Chem. Mater. 19 (2007) 374.
[15] L. Mai, B. Hu, W. Chen, Y. Qi, C. Lao, R. Yang, Y. Dai, Z.L. Wang, Adv. Mater. 19 (2007) 3712.
[16] V.S. Reddy, E.H. Walker Jr., C. Wen, S. Mho, J. Power Sources 183 (2008) 330.
[17] L.C. Yang, Q.S. Gao, Y. Tang, Y.P. Wu, R. Holze, J. Power Sources 179 (2008) 357.
[18] A.C. Dillon, A.H. Mahan, R. Deshpande, P.A. Parilla, K.M. Jones, S. Lee, Thin Solid Films 516 (2008) 794.
[19] S.H. Lee, Y.H. Kim, R. Deshpande, P.A. Parilla, E. Whitney, D.T. Gillaspie, K.M. Jones, A.H. Muhan, S. Zhang, A.C. Dillon, Adv. Mater. 20 (2008) 3627.
[20] L.C. Yang, Q.S. Gao, Y.H. Zhang, Y. Tang, Y.P. Wu, Electrochem. Commun. 10 (2008) 118.
[21] J.J. Auborn, Y.L. Barberio, J. Electrochem. Soc. 134 (1987) 638.
[22] J.R. Dahn, W.R. McKinnon, Solid State Ionics 23 (1987) 1.
[23] H.J. Fecht, Nanostruct. Mater. 6 (1995) 33.
[24] C.C. Koch, Nanostruct. Mater. 9 (1997) 13.
[25] A.V. Chadwick, S.L.P. Savin, Solid State Ionics 177 (2006) 3001.
[26] J. Li, L. Christensen, M.N. Obrovac, K.C. Hewitt, J.R. Dahn, J. Electrochem. Soc. 155 (2008) A234.
[27] J. Li, H.M. Dahn, L.J. Krause, D.B. Le, J.R. Dahn, J. Electrochem. Soc. 155 (2008) A812.
[28] M. Binnewies, E. Mike, Thermochemical Data of Elements and Compounds, Wiley-VCH, Weinheim, New York, 1999.
[29] H. Li, P. Balaya, J. Maier, J. Electrochem. Soc. 151 (2004) A1878.
[30] D. Larcher, L.Y. Beaulieu, D.D. MacNeil, J.R. Dahn, J. Electrochem. Soc. 147 (2000) 1658.
[31] D. Larcher, L.Y. Beaulieu, O. Mao, A.E. George, J.R. Dahn, J. Electrochem. Soc. 147 (2000) 1703.
[32] M.D. Fleischauer, M.N. Obrovac, J.D. McGraw, R.A. Dunlap, J.M. Topple, J.R. Dahn, J. Electrochem. Soc. 153 (2006) A484.
[33] K.T. Lee, Y.S. Jung, J.Y. Kwon, J.H. Kim, S.M. Oh, Chem. Mater. 20 (2008) 447.
[34] Y.S. Jung, K.T. Lee, J.H. Kim, J.Y. Kwon, S.M. Oh, Adv. Funct. Mater. 18 (2008) 3010.
[35] S. Laruelle, S. Grugeon, P. Poizot, M. Dollé, L. Dupont, J.-M. Tarascon, J. Electrochem. Soc. 149 (2002) A627.
[36] R. Debryvére, S. Laruelle, S. Grugeon, P. Poizot, D. Gonbeau, J.-M. Tarascon, Chem. Mater. 16 (2004) 1056.
[37] J. Jamnik, J. Maier, Phys. Chem. Chem. Phys. 5 (2003) 5215.
[38] Y.F. Zhukovski, P. Balaya, E.A. Kotomin, J. Maier, Phys. Rev. Lett. 96 (2006) 058302.
[39] J. Maier, Nat. Mater. 4 (2005) 805.
[40] G. Sudant, E. Baudrin, D. Larcher, J.-M. Tarascon, J. Mater. Chem. 15 (2005) 1263.
[41] M. Okubo, E. Hosono, J. Kim, M. Enomoto, N. Kojima, T. Kudo, H. Zhou, I. Honma, J. Am. Chem. Soc. 129 (2007) 7444.
[42] O. Delmer, P. Balaya, L. Kienle, J. Maier, Adv. Mater. 20 (2008) 501.
[43] G. Binotto, D. Larcher, A.S. Prakash, R.H. Urbina, M.S. Hegde, J.-M. Tarascon, Chem. Mater. 19 (2007) 3032.
[44] J.H. Ryu, J.W. Kim, Y.E. Sung, S.M. Oh, Electrochem. Solid-State Lett. 7 (2004) A306.
[45] Y.S. Jung, K.T. Lee, J.H. Ryu, D. Im, S.M. Oh, J. Electrochem. Soc. 152 (2005) A1452.
[46] Y.S. Jung, K.T. Lee, S.M. Oh, Electrochim. Acta 52 (2007) 7061.